Real-time temperature field measurement based on acoustic tomography

Real-time temperature field measurement based on acoustic tomography

Yong Bao, Jiabin Jia and Nick Polydorides

Institute for Digital Communications, School of Engineering, University of Edinburgh, Edinburgh, EH9 3FG, UK

Email: y.bao@ed.ac.uk, Jiabin.Jia@ed.ac.uk, N.Polydorides@ed.ac.uk

Abstract

Acoustic tomography can be used to measure temperature field from the time-of-flight (TOF). In order to capture real-time temperature field change and accurately yield quantitative temperature image, two improvements on the conventional acoustic tomography system are studied: simultaneous acoustic transmission and TOF collection along multiple ray paths, and offline iteration reconstruction algorithm. In system operation, all the acoustic transceivers send the modulated and filtered wideband Kasami sequence simultaneously to facilitate fast and accurate TOF measurements using cross-correlation detection. For image reconstruction, iteration process is separated and executed offline beforehand to shorten computational time for online temperature field reconstruction. The feasibility and effectiveness of the developed methods are validated in simulation study. Simulation results show that the proposed method can reduce the processing time per frame from 160 ms to 20 ms, and the reconstruction error remains less than 5%. Hence the proposed method has the potential of monitoring rapid temperature change with good temporal and spatial resolution.

Keywords: acoustic tomography, real-time temperature field reconstruction, offline iteration, Kasami sequence

1. Introduction

To improve the understanding of the combustion process and to evaluate the combustion efficiency, a great demand has been growing for an advanced measurement technique to measure real-time temperature inside the sensing area. There are a large number of efforts in developing robust and accurate temperature measurement techniques. Thermocouples are the mostly used devices but they have the drawbacks including intrusive, single-point sensing and corrosion in harsh environment. For the non-intrusive methods, laser based techniques, including Rayleigh scattering technique with aid of particle image velocimetry and laser Doppler velocimetry, has the disadvantage of being expensive and difficult to implement. Passive optical tomography with multi-camera tomography systems is able to provide non-invasive 3D flame monitoring and characterisation on laboratory scale furnaces with good spatial resolution. However, it also requires the object to be luminous and translucent in order to get the side view measurements [1]. Compared to other measurement techniques, acoustic tomography is one of few that can deliver accurate quantitative reconstruction of the whole temperature field with lower equipment cost.

Early application of acoustic tomography for monitoring temperature and wind velocity, was proposed in 1990 by Spiesberger [2] and in 1994 by Wilson and Thomson [3]. Later, imaging the near ground air temperature and wind flow with acoustic tomography was demonstrated in field experiments [3, 4], then extended to industrial applications like temperature field reconstruction [5-7].

Acoustic tomography uses the Time-Of-Flight (TOF) of sound to derive temperature image, because the sound speed in the sensing area is affected by the temperature of the intervening medium. The major challenge to employ acoustic tomography for real-time monitoring is the reconstruction accuracy and temporal resolution. In order to capture the dynamical changing temperature field and at the same time give accurate quantitative temperature reconstruction, processing time of TOF measurements and reconstruction computational time should be reduced.

In this paper, simultaneous TOF transmission and collection, and offline iteration reconstruction methods are studied to accelerate multichannel TOF measurement and online image reconstruction. Firstly, all the acoustic transceivers send the modulated and filtered wideband Kasami sequence simultaneously to facilitate fast and accurate TOF measurement using cross-correlation detection. Secondly, offline iteration reconstruction technique using smooth filter (OIRTF) is employed to improve image reconstruction. Unlike the conventional reconstruction algorithm, the iterative calculation is divided into two steps. The first one is independent from TOF measurement so that it can be calculated beforehand iteratively for high image quality. The second one is dependent on TOF, which should be calculated online non-iteratively for real-time

monitoring. Numerical simulations have been carried out to validate the performance of the proposed methods.

2. Methodology

2.1. Acoustic tomography

Simulation setup of the acoustic tomography system used in furnace is illustrated in figure 1. 16 acoustic transceivers are uniformly placed around the boundary of the sensing area to measure the TOF in 120 transceiver pairs. The sensing area with 1 m radius is divided into 1296 5 cm x 5 cm square pixels in reconstruction process.

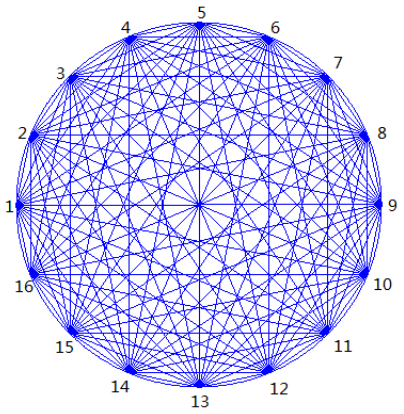

Figure 1. Acoustic tomography setup with 16 acoustic transceivers and 120 straight rays

Tomographic reconstruction is to firstly obtain the Laplace's sound speed, which is associated with temperature distribution, then corresponding temperature distribution can be calculated from the TOFs by solving a tomographic inverse problem. It has been mathematically proven that TOFs are sufficient to reconstruct the correct temperature field [8].

The forward problem of acoustic tomography is to define the relationship between TOFs and sound speed. Instead of modelling the forward problem using the wave equation, travel-time tomography employs the principles of geometrical acoustics to reconstruction sound speed distribution [9]. For finite bandwidth sound waves used for imaging, it is assumed that energy travels from the transmitter to the receiver along a ray path [10].

For the typical furnaces environment, the refraction effect of sound propagation will affect the accuracy of the tomographic reconstruction. However, according to Green's research on the acoustic tomography measurement error for temperature field in combustion gas [11], in the worst case, refraction effects cause about 2% reconstruction error. Therefore, a straight ray model, where the acoustic signal travels along a straight line between transmitter and receiver, is often used in acoustic tomography for simplicity [12-14].

Based on the straight ray model, TOF is defined as:

$$\tau = \int_{\Gamma} \frac{ds}{c_{eff}} \quad (1)$$

where τ is the TOF measurement, ds is the path element along ray Γ, and c_{eff} is the effective sound speed along the path element. c_{eff} is composed of a temperature dependent component, the Laplace's sound speed $c_L(T)$ and the flow dependent component, the flow velocity in the direction of sound propagation v.

$$c_{eff}(T, v) = c_L(T) + v \quad (2)$$

Reciprocal sound transmission is employed in acoustic tomography system. The average of these reciprocal travel times is used to reconstruct $c_L(T)$, so that the small effect from flow velocity v can be ignored. As described in equation (3), the approximation is valid since v^2 is much smaller than $c_L^2(T)$ in the furnace.

$$\begin{aligned} \tau_+ + \tau_- &= \int_{\Gamma} \frac{ds}{c_L(T) + v} + \int_{\Gamma} \frac{ds}{c_L(T) - v} \\ &= \int_{\Gamma} \frac{2c_L(T)\, ds}{c_L^2(T) - v^2} \\ &\approx \int_{\Gamma} \frac{2\, ds}{c_L\,(T)} \end{aligned} \quad (3)$$

Apply equation (3) to equation (1) then the forward problem can be modified as:

$$\frac{\tau_+ + \tau_-}{2} = l_\Gamma = \int_{\Gamma} \frac{ds}{c_L(T)} \quad (4)$$

Then equation (4) can be discretised as:

$$l_{\Gamma_i} = \sum_{j=1}^{N} a_{i,j} s_j \quad (5)$$

where l_{Γ_i} is the average of reciprocal travel times along i-th ray path, $s_j = \frac{1}{c_{L,j}(T)}$ is defined as the slowness in j-th pixel, $a_{i,j}$ is the segment length for each ray path across one pixel, $N = 1296$ is the total pixels number of an image.

The inverse problem of acoustic tomography is to reconstruct the slowness distribution s from the average of these reciprocal travel times l_Γ based on equation (5). Equation (5) is not accurate. The inaccuracy is incurred by the discretization using a coarse mesh grid, and the ignorance of refraction effect and flow velocity effect. The details of the reconstruction algorithm will be given in section 2.3.

The Laplace's sound speed depends on temperature T and properties of the medium, as defined in equation (6).

$$c_L = \frac{1}{s} = \sqrt{R\gamma T} \quad (6)$$

where $R = 287\ J\ kg^{-1}\ K^{-1}$ is the gas constant and specific heat ratio $\gamma = 1.4$ assuming gas composition is nearly constant in dry air.

Generally, in acoustic tomography the straight ray model is applied in the forward problem, then reciprocal tomography is used to obtain the average TOF along

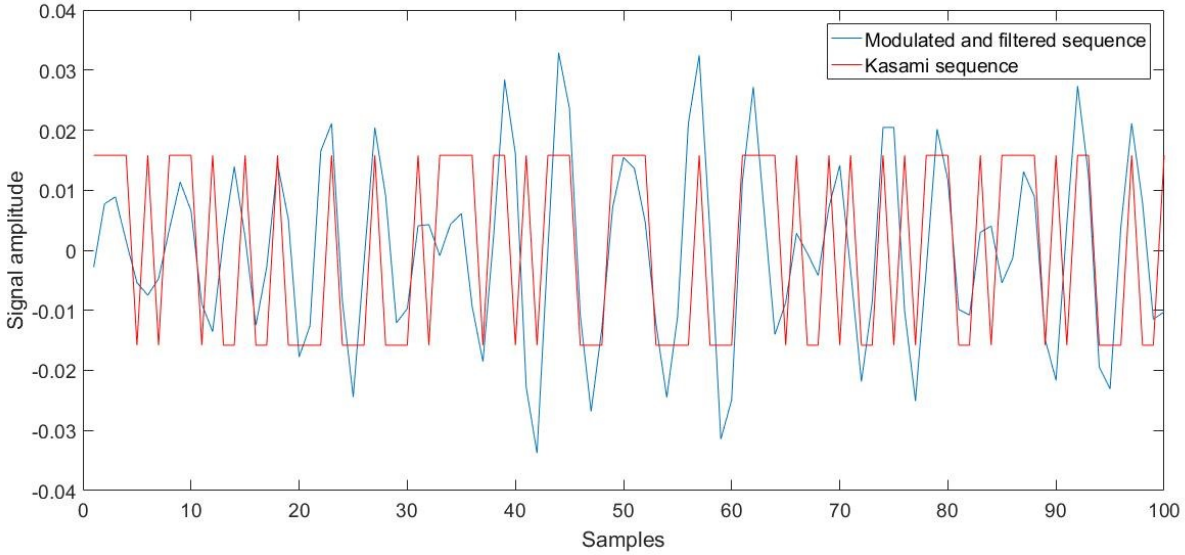

Figure 2. Kasami sequence (red) and the output signal (blue) after modulation and band-pass filter.

each ray path. Therefore the effect on the sound speed caused by the flow velocity can be ignored and the average TOF is the longitudinal line integral of Laplace's sound speed $c_L(T)$. By solving the inverse problem, $c_L(T)$ is reconstructed. Finally, the corresponding temperature distribution is calculated based on equation (6).

2.2. Simultaneous transmission and TOF measurement

In conventional acoustic tomography system, each transceiver is switched on sequentially to transmit acoustic signals to the receivers. That approach is easy to be implemented and has small interference for TOF detection as acoustic signals from different sources are separated in different time slot at the receiver. However, the temporal resolution of the system is sacrificed and it may not able to capture the dynamic temperature changes in the sensing area.

In the real-time acoustic tomography system, all the acoustic transceivers transmitting and receiving acoustic signals simultaneously. As a result, the measuring time is significantly reduced compared to the pairwise sequential measurement strategy. In this operation, each received signal is a summation of all other 15 delayed source signals.

$$y_j(t) = \sum_{i=1}^{16} x_i(t - \Delta t_{i,j}) + n_j(t) \text{ , i} \neq \text{j} \quad (7)$$

where $y_j(t)$ refers to the received signal at j-th receiver, $x_i(t)$ is the source signal from i-th transmitter and $\Delta t_{i,j}$ represents their corresponding delay time, which is the TOF in i-th ray path. $n_j(t)$ is the local noise received at j-th receiver.

The summed source signals must be separated at the receiver first, then their individual delay time $\Delta t_{k,j}$ can be estimated based on the cross-correlation detection defined as below.

$$R_{y_j x_k}(l) = \sum_{l=-\infty}^{+\infty}\left[y_j(t)x_k(t-l)\right] = \sum_{l=-\infty}^{+\infty}\left[\left[\sum_{i=1,i\neq j}^{16} x_i\left(t-\Delta t_{i,j}\right) + n_j(t)\right]x_k(t-l)\right]$$
$$= \sum_{i=1,i\neq j,i\neq \mathrm{k}}^{16} R_{x_i x_k}\left(l-\Delta t_{i,j}\right) + R_{x_k x_k}\left(l-\Delta t_{k,j}\right) + R_{n_j x_i}(l) \quad (8)$$

where l denotes the correlation delay and noise term $n_j(t)$ is uncorrelated with the source signal x_i, and x_k is the k-th reference signal waveform for cross-correlation detection.

In order to minimise the interference term $\sum_{i=1,i\neq j,i\neq \mathrm{k}}^{16} R_{x_i x_k}(l-\Delta t_{i,j})$ and noise term $R_{n_j x_k}(l)$, all the source signal waveforms should have good correlation property, such as sharp auto-correlation peak, but low cross-correlation value, for arbitrarily random delay $\Delta t_{i,j}$ and uncorrelated to the noise at the receiver.

Maximum Length Sequence (MLS) has a good asynchronous orthogonal property, which could be used to separate different source signals with arbitrary delay at the receiver. However, when a large number of simultaneous acoustic sources have to be used, like 16 in this case, the cross-correlation property of MLS is relatively poor. Selecting and combining the preferred pairs of MLS together can improve cross-correlation property, like the Kasami sequence. In fact, the Kasami sequence has near optimal cross-correlation values close to the Welch lower bound.

Therefore, the Kasami sequence shown in figure 2 is selected to generate acoustic signals for source signal separation and TOF detection. However, it is difficult to practically generate and transmit the Kasami sequence

with the acoustic transceivers, because the spectrum of the Kasami sequence is arbitrarily wide with sharp edges and discontinuity in time domain, but the transceiver is restricted to a limited bandwidth around a certain frequency. Therefore, before transmission, it is necessary to modulate the Kasami sequence with fixed carrier frequency, then a band-pass filter is used to smooth the Kasami sequence and control its bandwidth.

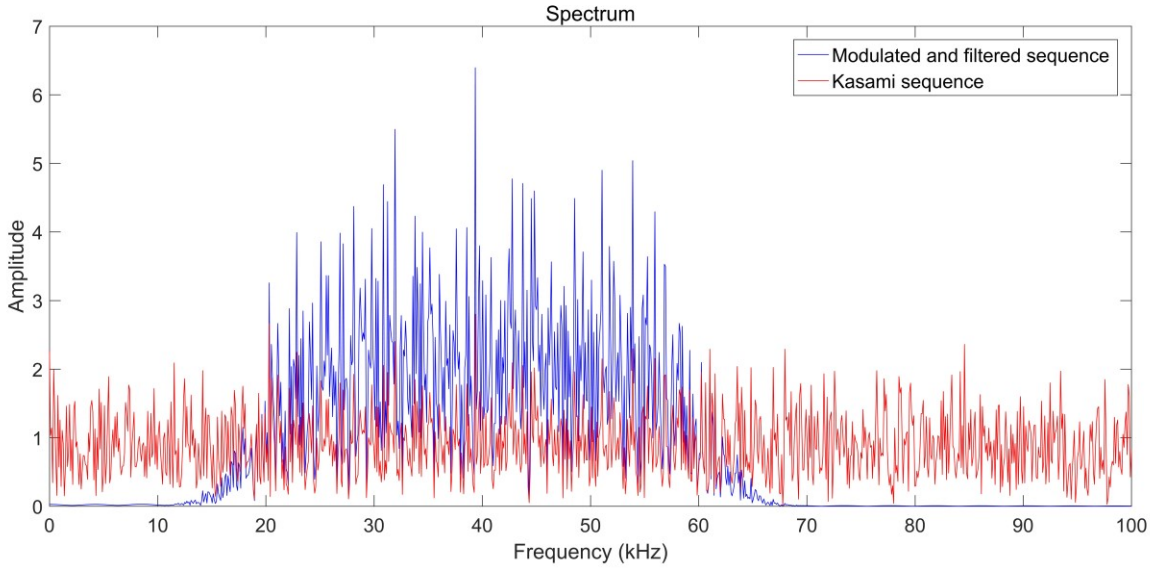

Figure 3. Kasami sequence (red) and modulated and filtered output sequence (blue) in frequency domain. After modulation and band-pass filter, the bandwidth of output signal is limited and centred at the 40 kHz carrier frequency.

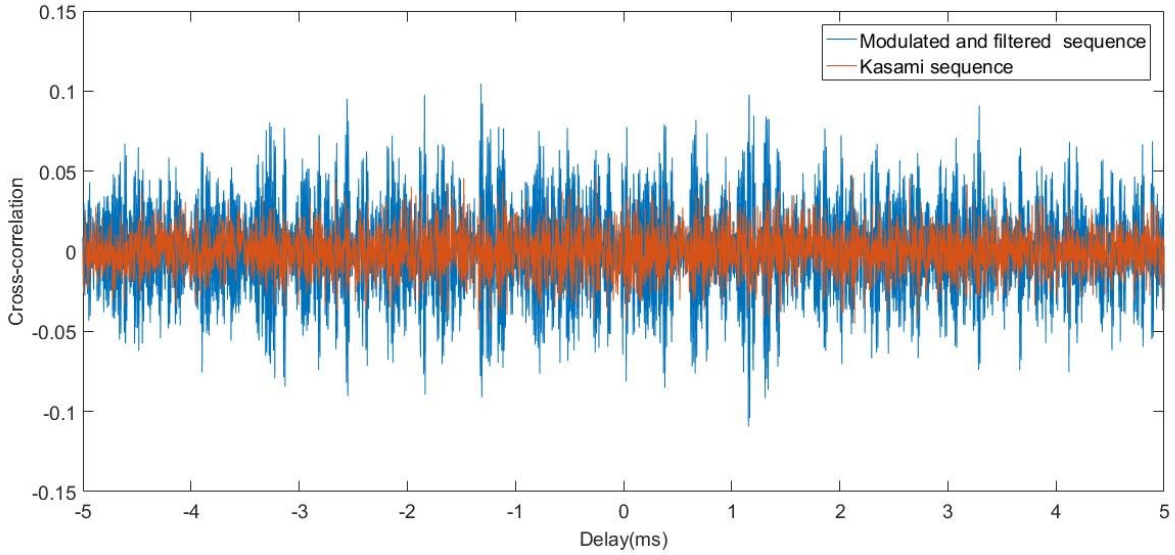

Figure 4. Cross-correlation of Kasami sequence (red) and modulated and filtered sequence output (blue). The cross-correlation value of the filtered sequence is much larger than the Kasami sequence, which results in a larger interference in TOF detection.

As shown in figure 3, compared with the original Kasami sequence, the modulated and filtered Kasami sequence has a narrower bandwidth, which can meet the transmission requirement for acoustic transceivers. However, modulation and filtering will also weaken the correlation property of waveform. The auto- and cross-correlation comparison is given in figure 4 and 5 respectively. The auto-correlation coefficients of the filtered Kasami sequence is a smoothed version of the original correlation of Kasami sequence. The auto-correlation peak value is reduced while the cross-correlation value, which can be considered as the interference in TOF detection, is increased. Once the interference and noise overwhelms the auto-correlation peak value, it is impossible to detection accurate travel-time delay from the received signal. Besides, at the receiver, it is difficult to build an inverse filter to remove the smooth effect, as many zeros exist in the impulse response of the band-pass filter. The only way to enhance the auto-correlation property is to increase the length of Kasami sequence and produce a sharp auto-correlation peak. Meanwhile a good temporal resolution must remain for the acoustic tomography system. The selection of the parameters of Kasami sequence will be discussed in section 3.2.

In summary, in order to improve the temporal resolution of TOF measurement, the wideband acoustic signal waveform is designed based on modulated and filtered Kasami sequence, which allows simultaneous signal transmission and data collection from all the acoustic ray paths. Then accurate TOF measurements along each ray path can be calculated by correlation detection.

2.3. Temperature field reconstruction

The inverse problem of acoustic tomographic is to reconstruct the slowness s distribution from a limited number of TOF measurements, as defined in equation (4). There are two major difficulties associated with this inverse problem. Firstly, it is under-determined because the number of unknowns $\mathrm{N} = 1296$ (the number of pixels) is much larger than the number of equations $\mathrm{M} = 120$ (the number of TOF measurements). Therefore, the solution is not unique. Secondly, equation (4) is an integral equation, which is ill-posed, and its corresponding discrete form, equation (5), is ill-conditioned. This means that the solution of equation (5) is sensitive to small perturbations in TOF measurements.

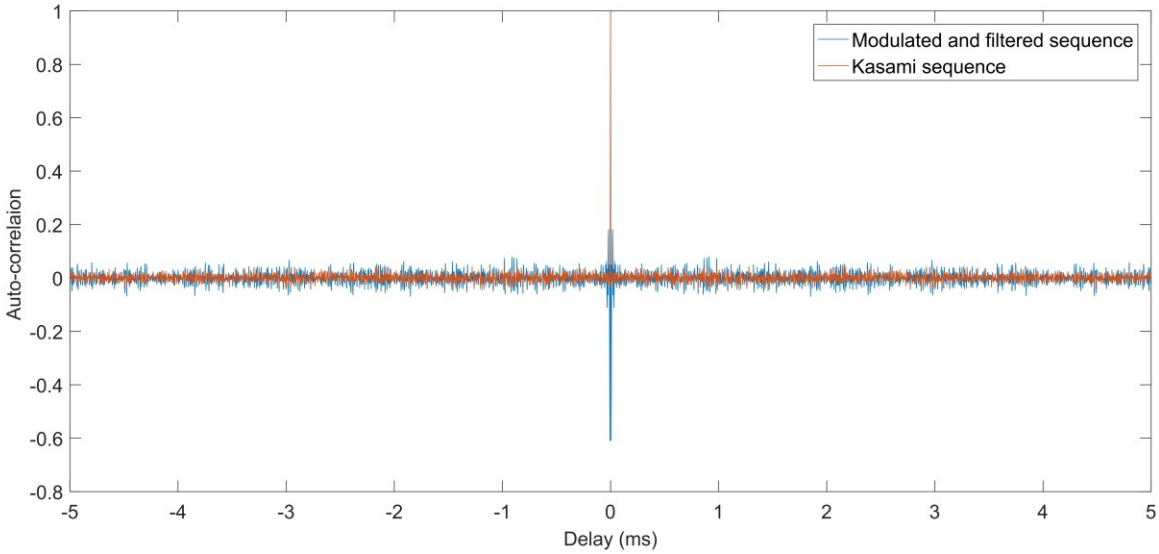

Figure 5. Auto-correlation of Kasami sequence (red) and modulated and filtered output sequence (blue). The auto-correlation of the filtered sequence has larger sidelobes and lower peak value than that of the Kasami sequence.

Numerous algorithms are available to solve the inverse problem. These algorithms can be categorised into three main branches including algebraic-based algorithms [8, 15, 16], sparse reconstruction framework [12-14] and stochastic-based algorithms [3, 7, 17-19].

Among these algorithms, sparse reconstruction framework assumes that the temperature distribution can be represented as a linear combination of some kernel functions (e.g., set of different bases) where most of the coefficients are zero. Stochastic-based method assumes that the sensing field is statistically homogeneous in space. Without much prior knowledge, it is difficult to apply these methods for arbitrary temperature or velocity field. Algebraic-based algorithm is used in our study for real-time image reconstruction.

2.3.1. Conventional reconstruction methods

Algebraic-based algorithms are conventional image reconstruction methods. A number of new or different algorithms have been developed to address the under-determined and ill-conditioned inverse problems using non-iterative (i.e. single step) algorithms and iterative algorithms.

Non-iterative algorithms include the Linear Back Projection (LBP) method, Standard Tikhonov Regularisation (STR) method and subspace projection method [6, 20, 21]. Usually LBP and STR suffer from low imaging accuracy. The reconstruction performance of the subspace projection method heavily relies on the selection of basis function, because the dominant features of slowness distribution can be represented by a low-dimension basis function. Weighted Radial Basis Functions (RBF) are popular in subspace projection methods but the approximation error of RBF increases due to perturbations of the temperature field. Moreover, this projection typically leads to a rank deficient inverse problem and it amplifies the noise in TOF measurements.

For iterative algorithm, an upgrade of Simultaneous Iterative Reconstruction Technique (SIRT) algorithm was applied by Ziemann [4] to solve the inverse problem for acoustic tomography system. This algorithm is favoured for its fast convergence and stability. Generally, it is defined as follow:

$$s_j^{t+1} = s_j^t + \frac{\alpha}{\sum_{i=1}^{M} a_{i,j}} \sum_{i=1}^{M} \frac{a_{i,j}(\tau_i - \sum_{j=1}^{N} a_{i,j} s_j^t)}{\sum_{j=1}^{N} a_{i,j}} \qquad (9)$$

where τ_i is the element of TOF measurement along i-th ray path. s_j^t is the element of slowness in j-th pixel in t-

th iteration, $a_{i,j}$ is the segment length for each ray path across one pixel, α is the constant iteration step size, N is the total number of the pixels (1296) and M is the number of measurement (120).

The k-th iteration can be rewritten in a matrix form as

$$\boldsymbol{s}^{k+1} = \boldsymbol{s}^k + \alpha \boldsymbol{D_p}(\boldsymbol{D_r A})^T(\boldsymbol{\tau} - \boldsymbol{A s}^k) \qquad (10)$$

where

$$\boldsymbol{D_p} = \mathrm{diag}(1/LP_1, 1/LP_2, \dots, 1/LP_N)$$
$$\boldsymbol{D_r} = \mathrm{diag}(1/LR_1, 1/LR_2, \dots, 1/LR_M) \qquad (11)$$

$LP_j = \sum_{i=1}^{M} a_{i,j}$ and $LR_i = \sum_{j=1}^{N} a_{i,j}$. α is set as 1for the conventional SIRT in equation (9). A is the matrix containing all $a_{i,j}$. Recent research showed the reconstruction performance depended on the appropriate iteration step size [22]. The optimal step size will be discussed in equation (15) and equation (16).

LP_j is the segment total length for all the ray paths across j-th pixel and $\boldsymbol{D_p}$ is the diagonal preconditioner which is used to geometrically weight the least square cost function**.** LR_i is the length of i-th ray path and $\boldsymbol{D_r}$ is the normalised operator to make sure that the sum of each row of A equals to 1. By weighting $\boldsymbol{D_r}$, when residual norm is minimised, the rays that intersect larger portions of image can tolerate larger errors than the rays that are much shorter.

2.3.2. Regularisation and iteration step size

The iterative reconstruction algorithm described above does not guarantee a correct unique solution, as the inverse problem itself is very ill-posed. The conventional way to deal with ill-posed problem is to add a regularisation term in the reconstruction cost function [23]. For most cases, Tikhonov regularisation is used. The iteration correction using Tikhonov regularisation is

$$\boldsymbol{s}^{k+1} = \boldsymbol{s}^k + \alpha \boldsymbol{D_p}(\boldsymbol{D_r A})^T\left(\boldsymbol{\tau} - \boldsymbol{A s}^k\right) + \eta \boldsymbol{\Gamma}^T \boldsymbol{\Gamma} \boldsymbol{s}^k \quad (12)$$

where η is the regularisation parameter and $\boldsymbol{\Gamma}$ is the regularisation matrix.

In addition to the Tikhonov regularisation method, the projection operator is also used to improve the convergence rate and stabilise the solution, mostly in space domain based on a fixed or adaptive threshold.

However, space domain projection is not suitable for the offline iteration reconstruction method, because the projection operator is not linear and the results depend on measurements. Moreover, it is difficult to choose an optimal fixed threshold for unpredictable changes in the temperature field. To solve this problem, a smooth filter is applied, which can be considered as a frequency domain projection, assuming that the temperature field is generally smooth.

The iteration correction using the smooth filter operator is defined as

$$\boldsymbol{s}^{k+1} = \boldsymbol{\mathcal{P}}(\boldsymbol{s}^k + \alpha \boldsymbol{D_p}(\boldsymbol{D_r A})^T(\boldsymbol{\tau} - \boldsymbol{A s}^k)) \qquad (13)$$

Both $\boldsymbol{\Gamma}$ in Tikhonov regularisation and $\boldsymbol{\mathcal{P}}$ in smooth filter operator can be defined by a 2D Gaussian low-pass filter

$$G(x, y) = \frac{1}{2\pi\sigma^2} e^{-\frac{x^2+y^2}{2\sigma^2}} \qquad (14)$$

where x and y are coordinates, and σ is the variance controlling the shape of the Gaussian kernel.

The convergence analysis of regularised SIRT was given by Jiang [24]. The near-optimal fixed step size α was studied by Gregor and Fessler [22].

For the additive Tikhonov regularised case, the iteration step size α is

$$\alpha = \frac{2}{1+\frac{tr(\boldsymbol{D_p A^T D_r A})}{N}+\eta\left(\frac{1}{\min_j LP_j}+\frac{1}{\max_j LP_j}\right)} \qquad (15)$$

For the filtered regularised case, the iteration step size α is

$$\alpha = \frac{2}{\lambda_{min}+\lambda_{max}} = 2 \qquad (16)$$

where λ_{min} and λ_{max} mean the smallest and largest Eigen value of matrix $\boldsymbol{\mathcal{P} D_p A^T D_r A}$, $\lambda_{max} = 1$ as a result of preconditioning and $\lambda_{min} = 0$ for the matrix that has no full column rank.

2.3.3. Offline iteration method

In most real-time monitoring system, non-iterative methods are preferred for fast reconstruction speed. To improve the accuracy of non-iterative method, many researchers tried to iteratively calculate the optimal inversion operator beforehand for non-iterative online reconstruction, for instance, Offline Iteration Online Reconstruction (OIOR) [25] based on Landweber iteration, and Direct Landweber (DLW) based on modified Landweber [26]. In order to build a real-time acoustic tomography system, the offline iteration method is applied based on the SIRT method defined in equation (12) and equation (13), named offline iteration reconstruction technique using Tikhonov regularisation (OIRTT) and smooth filter (OIRTF). Consequently, the processing time of online reconstruction can be reduced to the same level as non-iterative method like LBP.

The principle of this method is to design an iteration method, whose iteration procedure is linear and independent of measurement data, which means that the iteration of equation (12) and equation (13) can be rewritten as

$$\boldsymbol{s}^{\boldsymbol{k+1}} = \boldsymbol{B s}^{\boldsymbol{k}} + \boldsymbol{D\tau} \qquad (17)$$

where $\mathbf{B} = \left(\boldsymbol{I} - \boldsymbol{\alpha D_p}(\boldsymbol{D_r A})^T\boldsymbol{A} + \eta \boldsymbol{\Gamma}^T\boldsymbol{\Gamma}\right)$ and $\boldsymbol{D} = \boldsymbol{\alpha D_p}(\boldsymbol{D_r A})^T$ for OIRTT, and $\boldsymbol{B} = \boldsymbol{\mathcal{P}}(\boldsymbol{I} - \boldsymbol{\alpha D_p}(\boldsymbol{D_r A})^T\boldsymbol{A})$ and $\boldsymbol{D} = \boldsymbol{\alpha \mathcal{P} D_p}(\boldsymbol{D_r A})^T$ for OIRTF.

For the purpose of reconstruction independent of measurement data, the solution $\boldsymbol{s}^{\boldsymbol{k+1}}$ is decomposed into two part, iterative term $\boldsymbol{C}^{\boldsymbol{k+1}}$ and non-iterative term $\boldsymbol{\varepsilon}$

$$\boldsymbol{s^{k+1} = C^{k+1}\varepsilon} \quad (18)$$

Substituting equation (18) into equation (17)

$$\boldsymbol{C^{k+1}\,\varepsilon = BC^{k}\,\varepsilon + D\tau} \quad (19)$$

Let $\boldsymbol{\varepsilon = \tau}$, then the iterative term $\boldsymbol{C^{k+1}}$ is independent of TOF measurement $\boldsymbol{\tau}$ and can be calculated offline in advance using equation below.

$$\boldsymbol{C^{k+1} = BC^{k} + D} \quad (20)$$

Given the iteration number k, after $\boldsymbol{C}$ is iteratively obtained offline and all the TOF $\boldsymbol{\tau}$ is measured, the speed slowness $\boldsymbol{s}$ can be determined by equation (21). Finally, temperature is derived from equation (6).

$$\boldsymbol{s = C\tau} \quad (21)$$

For the offline iteration calculation of $\boldsymbol{C}$, its iteration number k need to be determined beforehand.

In summary, offline iteration reconstruction methods with Tikhonov regularisation (OIRTT) and smooth filter (OIRTF) are developed to improve online reconstruction speed of the real-time acoustic tomography system. These methods are able to iteratively calculate the inverse operator beforehand and reduce the online computational time to the same level of non-iterative algorithm. At the same time the reconstruction accuracy is close to the iterative methods. Iteration number k for offline iteration and type of regularisation term will be determined based on numerical simulation results described in section 3.3.

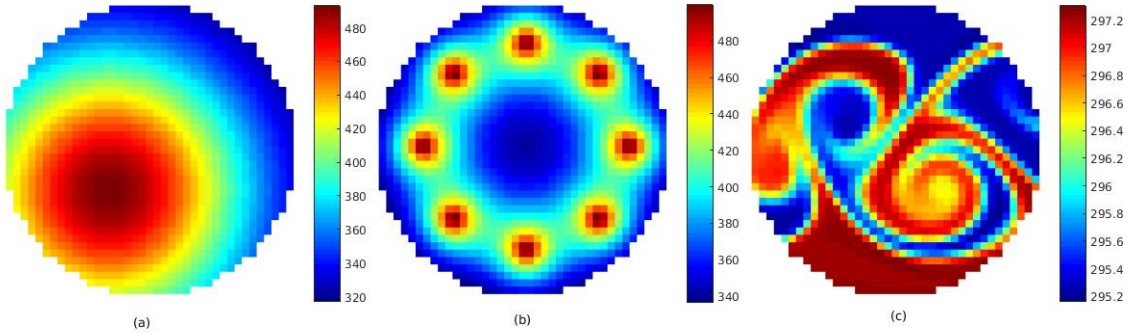

Figure 6. Temperature fields in the simulation (a) one heat source (b) multiple heat sources (c) turbulent flow

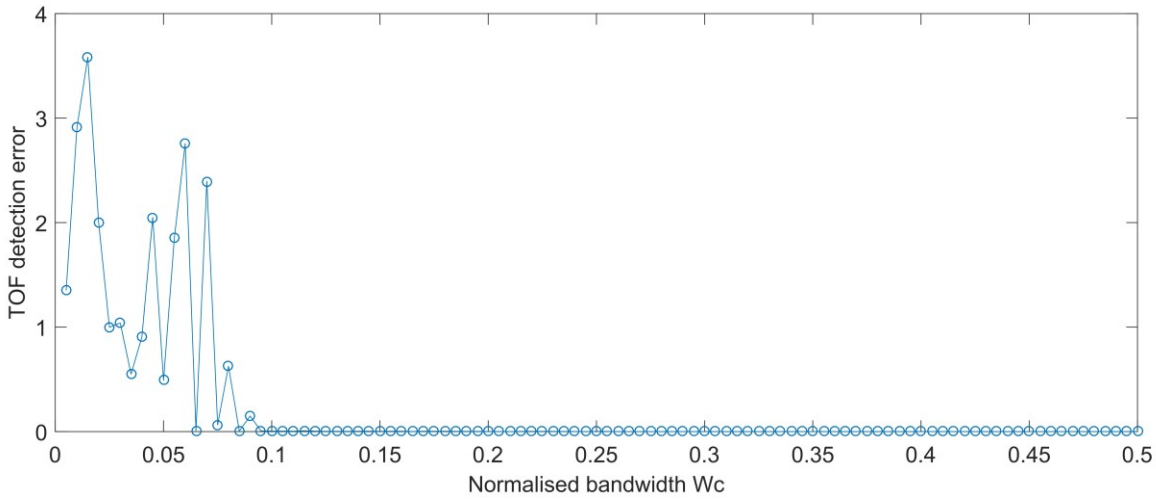

Figure 7. Change of TOF detection error with normalised band-pass filter bandwidth

3. Simulation results and discussions

3.1. Simulation setup

The forward problem of acoustic tomography is solved in Finite Element method simulation environment using COMSOL Multiphysics pressure acoustic module. The acoustic wave propagation is studied in an ideal isentropic process, where all the thermodynamic process is assumed reversible and adiabatic. The acoustic signal is considered as a longitudinal wave and a flow of energy with the rapid change above a static value. The governing equation below is based on the conservation of mass and momentum [27]

$$\frac{1}{\rho_0 c^2}\frac{\partial^2 P'}{\partial t^2} + \nabla \cdot \left(-\frac{1}{\rho_0}\nabla p'\right) = 0 \quad (22)$$

The small parameter expansion is performed on a stationary fluid with density ρ_0 and pressure p_0, such that $p = p_0 + p'$ and $\rho = \rho_0 + \rho'$. c is the sound speed.

In the forward model, the solution to acoustic problems is wavelike and the wave is characterised by a wavelength λ in space. According to the Nyquist's law,

there should be at least 2 samples per wavelength for discretisation. In this simulation 10 samples per wavelength is used. As the propagation direction is unknown beforehand, an isotropic free tetrahedral mesh is employed. The maximum element size is set as $\lambda/10$. The sensing area is divided into 1296 pixels, surrounded by 16 acoustic transceivers which give 120 TOF measurements per image. Figure 6 shows three different cases in simulation to verify the performance of the algorithms. In the first scenario, temperature field is simulated with one heat source. In the second one, multiple heat sources are set up. In the third scenario, temperature field is a turbulent flow, and the data come from Wiens's work [21].

3.2. TOF measurement

For the purpose of real-time measurement, the acoustic signal waveform is designed based on the modulated and filtered Kasami sequence. Correlation detection is used to estimate the TOF. In the simulation, all the transmitted signals reached the receivers with preset delay and the detection error change with the bandwidth of band-pass filter. The relation between TOF detection error and normalised bandwidth of band-pass filter (the ratio of the bandwidth of filter and the sampling frequency) is shown in figure 7. It is clear that, for the accuracy of TOF detection, the normalised bandwidth should be larger than 0.1, which means that the output signal bandwidth should be at least $1/10$ of the sampling frequency. As mentioned in section 2.2, there is a trade-off between Kasami sequence length and system temporal resolution. The bandwidth of output signal is 40kHz which requires that the sampling frequency to be 400kHz. As the TOF varying from 0.5 ms to 6 ms, these TOFs will cause 200 to 2400 samples delay in the receiver. In order to maintain a good cross-correlation property of the received signal with up to 2400 samples delay, the signal sequence length should be larger than 4000 samples, which means that the output signal last for 10 ms.

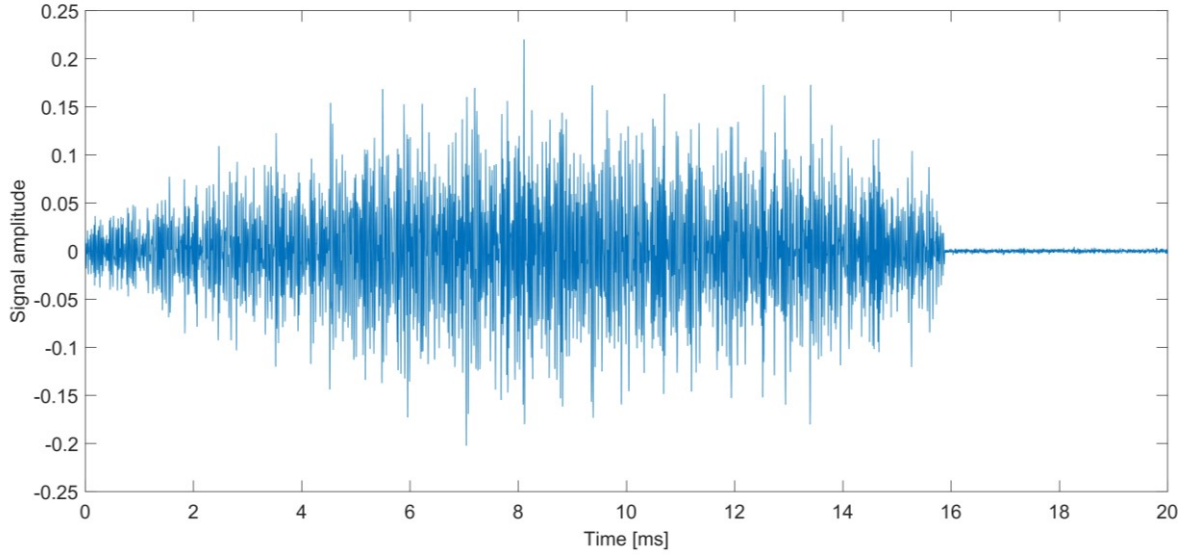

Figure 8: Received signal at one transceiver from all other 15 sources. All the transceivers send acoustic signals for 10ms. The measurement time for each image lasts for 20ms.

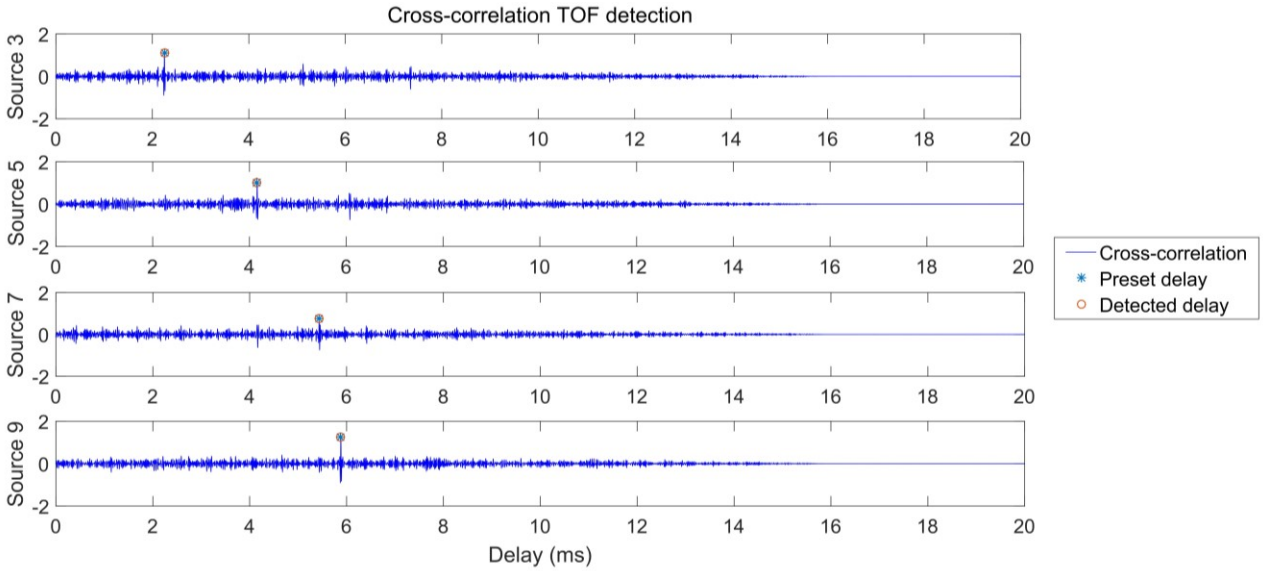

Figure 9. Cross-correlation TOF detection results from simulation. The preset delay is marked with '*' and the detected delay is marked in the red circles.

Generally, compared with the pairwise TOF measurement process, the length of the transmitted signal is increased from 5 ms to 10 ms and total measuring time for each transceiver pairs increase from 10 ms to 20 ms. However, because the total measuring time per frame is reduced from 160 ms to 20 ms, therefore the system speed is still improved from 6.25 frames per second to 50 frames per second. All the parameters of transmitted acoustic waveform is listed in table 1. An example of the received signal is showed in figure 8, which is the summation of all 15 sources. The cross-correlation detection of TOFs is showed in figure 9, where the arrival time of transmitted signal from the transceiver 1 to the transceiver 3, 5, 7 and 9 is indicated on the cross-correlation peaks. The overlaps between preset delay and detected delay demonstrate the very good accuracy of TOF detection.

Table 1. Parameters for generating acoustic waveform

Sampling frequency	400 kHz
Carrier frequency	40 kHz
Band-pass filter bandwidth	40 kHz
Filter normalised bandwidth	0.1
Filter length	81
Filter window	Kaiser
Total measurement time per image	20 ms
Pulse duration	10 ms
Kasami code polynomial	[14, 13, 8, 4, 0]

3.3. Reconstruction results

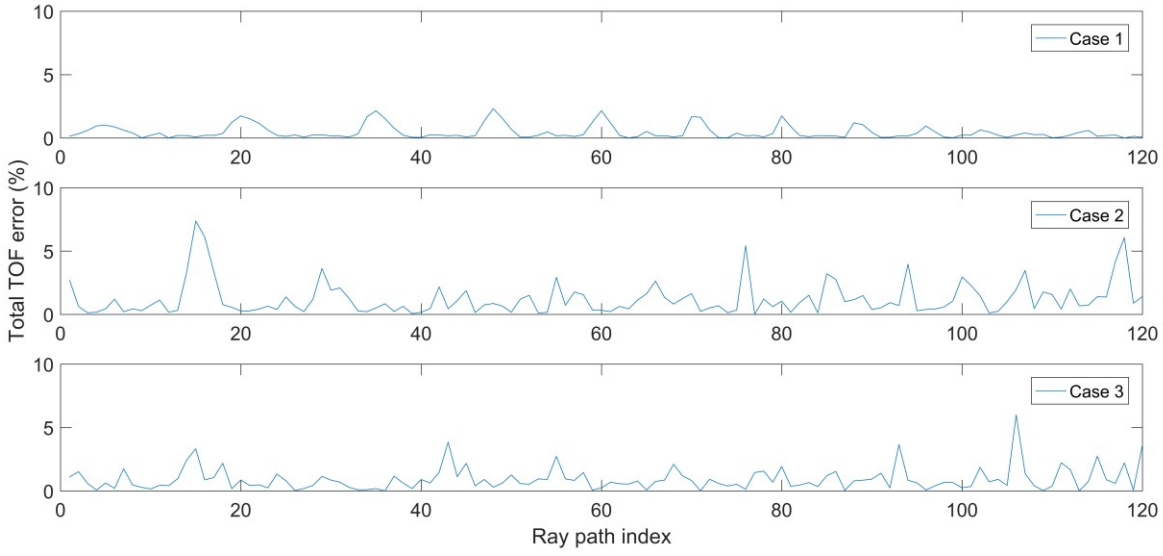

Figure 10. TOF errors of different ray paths in case 1, case 2 and case 3.

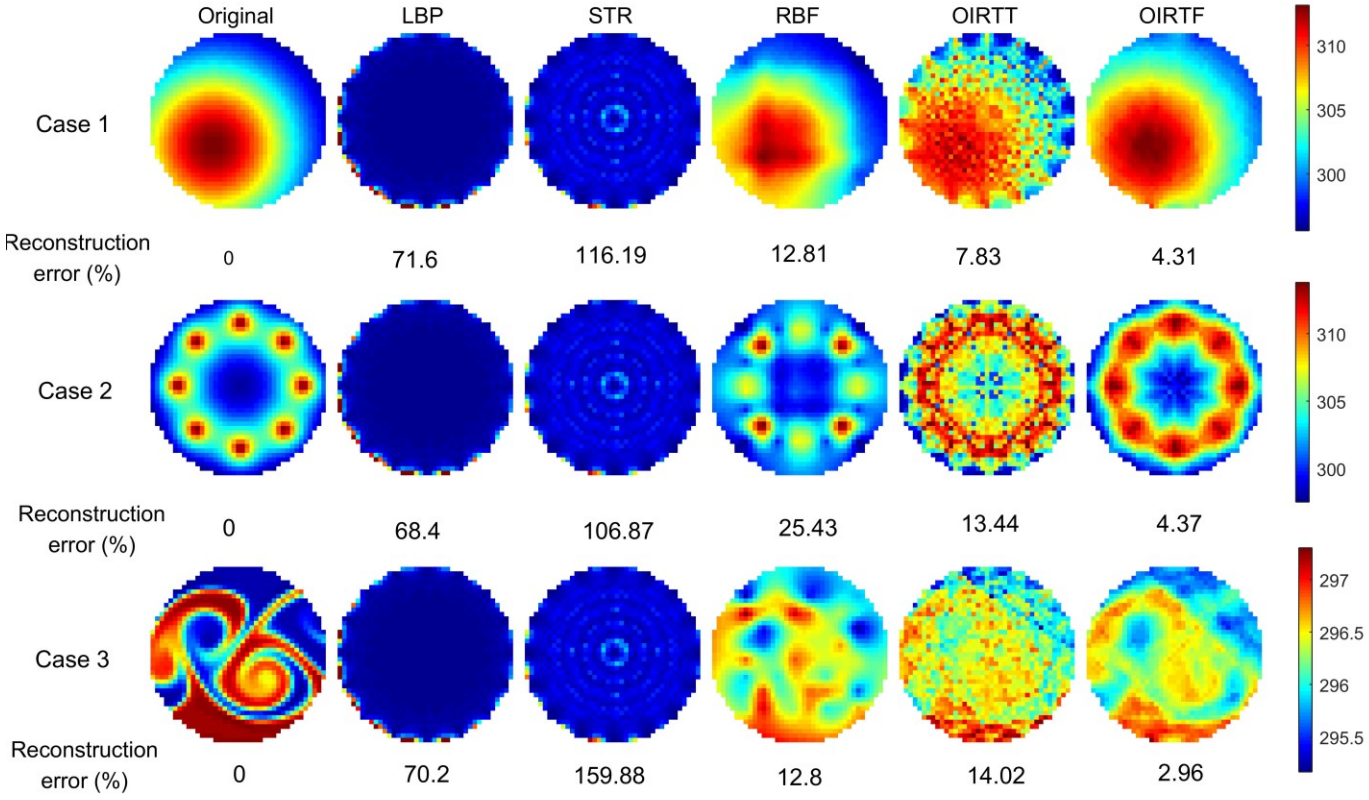

Figure 11. Simulation scenarios and reconstructed temperature fields using different algorithms. The reconstruction error (%) is shown beneath each image

The reconstruction process is to calculate sound speed distribution from TOF measurements based on equation (5). As mentioned in section 2.1, equation (5) is not accurate. The inaccuracy is incurred by the discretisation using a coarse mesh grid, and the ignorance of refraction effect and flow velocity effect. The inaccuracy of equation (5) will cause the modelling error. The difference between the longitudinal integrals l_Γ calculated from simulated TOFs and $\sum_{j=1}^{N} a_{i,j} s_j$, known as the total TOF error which contains both inaccuracy of the forward problem and TOF detection error, is defined in equation (23).

$$ef_i = \frac{\left(l_{\Gamma i} - \sum_{j=1}^{N} a_{i,j} s_j\right)^2}{{l_{\Gamma_i}}^2} \qquad (23)$$

The ef_i for three cases are given in figure 10. The TOF detection error of cross-correlation detection is much smaller than the modelling error, which can be ignored. Therefore the modelling error can be estimated from ef_i. The modelling error can be reduced by a non-linear acoustic tomography system which allows updating the ray path iteratively with the temperature field reconstruction. But this is not quite suitable for the real-time monitoring system. However, the average forward problem inaccuracy is 1.3%, 1.19% and 0.34% for three cases respectively, which means the equation (5) can still be used in reconstruction.

The performance of proposed algorithms, computational time and reconstruction error, is evaluated based on the simulated TOF measurements from the three cases shown in section 3.1. The OIRTT and OIRTF method is compared with other non-iterative reconstruction algorithms, i.e. LBP, standard Tikhonov regularisation (STR), subspace projection methods using RBF network [21].

Figure 11 shows the reconstruction performance of these non-iterative and offline iterative methods in all three cases. Image reconstruction error defined in equation (24) is employed to quantitatively compare different algorithms

$$e = \frac{\|T_{re} - T_{ori}\|^2}{\|T_{ori}\|^2} \qquad (24)$$

where T_{ori} stands for the original temperature values set in simulation and T_{re} represents the reconstructed temperature values.

Both LBP and STR are not able to give a good reconstruction of the temperature field. For the subspace projection methods, the reconstruction error can be split into two part, the approximation error of RBF modelling of the temperature field and the calculation error using Truncated Singular Value Decomposition (TSVD) to solve the inverse problem. In case 1 and 3 the temperature field is smooth with small fluctuation, which allows the RBF representation to catch the dominant features, therefore the image error is small. In the image reconstruction, as most energy is stored in the largest few SVD basis with respect to the number of largest singular values. TSVD method can help to remove the noise effect and reconstruct the original image. However in case 2, not only the image reconstruction error increases but also the calculation

error increases due to severe rank efficiency problem, which indicates that subspace projection method is not a good option for recovering image with sharp peaks and large fluctuation.

The iteration convergence rate of the offline OIRTT and OIRTF in figure 12 shows that smooth filter operator has slightly faster convergence rate than Tikhonov regularisation. In all three cases, the offline iteration number is 100 for both OIRTT and OIRTF. The regularisation parameter η in equation (12) is 0.005 and the Gaussian kernel variance σ in equation (14) is 1.

Generally, offline iteration methods has a better reconstruction performance compared to other non-iterative methods, especially in case 2 with a large variation of temperature distribution. Besides, in all three cases the reconstruction error of OIRTF is much smaller than OIRTT. One of possible reasons is that the smooth filter can be considered as frequency domain projection, and then the iterative calculation defined in equation (13) can be considered as a projected Landweber with preconditioning which helps to accelerate convergence. It follows from many numerical simulations and practical applications that this method can provide much better estimations than the usual linear regularisation methods [28].

The computational time of different reconstruction methods is compared in table 2. The specifications of the computer used for comparison are Intel(R) Xeon(R) CPU E5-1660 v3, 31.3 GB RAM, Scientific Linux 7.2 with MATLAB R2015b. The LBP method has the least computational cost since its reconstruction process is simplified as matrix multiplication. The RBF method uses TSVD to solve the inverse problem, where SVD decomposition can be calculated offline and only few singular values is used for reconstruction online. The STR method needs more computation time to calculate the pseudo inverse solution. As for OIRTF, about 4000 ms is spent on offline iteration beforehand, whereas online reconstruction only takes over 0.1 ms to reconstruct one temperature image, which is close to LBP. The computational time of OIRTT is similar to that of OIRTF.

In conclusion, to solve the ill-posed inverse problem, offline iteration reconstruction method with a filter regularisation is developed. The smooth filter operator is built based on a pre-defined Gaussian smooth kernel.

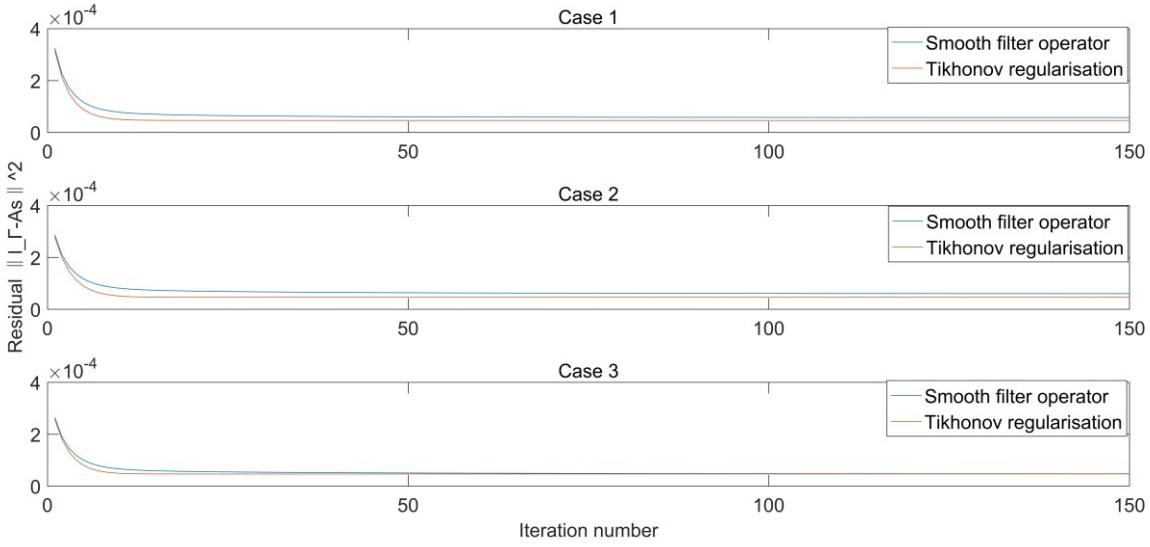

Figure 12: Offline iteration convergence rate of OIRTT(blue) and OIRTF(red)

Table 2. Computational time per temperature image of different reconstruction methods

Computational time (ms)	LBP	STR	RBF	OIRTF	
				Offline iteration	Online reconstruction
Case 1	0.09592	359.4	46.93	4012.3	0.1134
Case 2	0.05724	253.3	59.31	3910.7	0.1021
Case 3	0.03197	234.4	69.13	4142.2	0.1108

4. Conclusions

In this paper, two improvements on the conventional acoustic tomography system are studied for temperature field measurement: simultaneous acoustics signal transmission and time-of-flight (TOF) collection along multiple ray paths, and offline iteration reconstruction algorithm. In this mode of operation, TOF detection process for different paths is performed simultaneously based on cross-correlation detection. For image reconstruction, iterative reconstruction with the smooth filter operator is applied in an offline mode for accurate online temperature field reconstruction with good quantitative accuracy. Acoustic propagation in three temperature fields are simulated to evaluate imaging error and computational time. The results of feasibility study demonstrate that improved acoustic tomography can achieve 50 frames of temperature images per second with less than 5% reconstruction error.

References

1. Yan, Y., et al., *Recent advances in flame tomography.* Chinese Journal of Chemical Engineering, 2012. **20**(2): p. 389-399.
2. Spiesberger, J.L., et al., *Passive localization of calling animals and sensing of their acoustic environment using acoustic tomography.* American Naturalist, 1990: Vol. 135, no.1, pp.107-153.
3. Wilson, D., et al., *Acoustic tomographic monitoring of the atmospheric surface layer.* Journal of Atmospheric and Oceanic Technology, 1994. **11**(3): p. 751-769.
4. Ziemann, A., et al., *Acoustic tomography in the atmospheric surface layer*. in *Annales Geophysicae*. 1998. Springer Berlin/Heidelberg.
5. Schwarz, A., *Three - Dimensional Reconstruction of Temperature and Velocity Fields in a Furnace.* Particle & particle systems characterization, 1995. **12**(2): p. 75-80.
6. Li, Y. , et al., *Experimental study on acoustic vector tomography of 2-D flow field in an experiment-scale furnace.* Flow Measurement and Instrumentation, 2006. **17**(2): p. 113-122.
7. Liu, Y., et al., *A method for simultaneous reconstruction of temperature and concentration distribution in gas mixtures based on acoustic tomography.* Acoustical Physics, 2015. **61**(5): p. 597-605.
8. Jovanovic, I., *Inverse problems in acoustic tomography.* 2008 PhD thesis.
9. Hormati, A., et al. *Robust ultrasound travel-time tomography using the bent ray model*. in *Proc. SPIE*. 2010 Vol.7629.
10. Duric, N., et al. *Acoustic tomography: promise versus reality*. in *2011 IEEE International Ultrasonics Symposium*. 2011. IEEE.
11. Green, S. *Acoustic temperature and velocity measurement in combustion gases*. in *Eight International Heat Transfer Conference*. 1986.
12. Jovanovic, I., et al. *Efficient and stable acoustic tomography using sparse reconstruction methods*. in *19th International Congress on Acoustics*. 2007.
13. Dogan, Z., et al. *3D reconstruction of wave-propagated point sources from boundary measurements using joint sparsity and finite rate of innovation*. in *2012 9th IEEE International Symposium on Biomedical Imaging (ISBI)*. 2012. IEEE.
14. Toši, I., et al. *Ultrasound tomography with learned dictionaries*. in *2010 IEEE International Conference on Acoustics, Speech and Signal Processing*. 2010. IEEE.
15. Ziemann, A. , et al.,*Acoustic tomography as a remote sensing method to investigate the near-surface atmospheric boundary layer in comparison with in situ measurements.* Journal of Atmospheric and Oceanic Technology, 2002. **19**(8): p. 1208-1215.
16. Holstein, P., et al., *Acoustic tomography on the basis of travel-time measurement.* Measurement Science and Technology, 2004. **15**(7): p. 1420.
17. Vecherin, S.N., et al., *Time-dependent stochastic inversion in acoustic travel-time tomography of the atmosphere.* The Journal of the Acoustical Society of America, 2006. **119**(5): p. 2579-2588.
18. Vecherin, S.N., et al., *Tomographic reconstruction of atmospheric turbulence with the use of time-dependent stochastic inversion.* The Journal of the Acoustical Society of America, 2007. **122**(3): p. 1416-1425.
19. Kolouri, S. , et al., *Acoustic tomography of the atmosphere using unscented Kalman filter.* IEEE Transactions on Geoscience and Remote Sensing, 2014. **52**(4): p. 2159-2171.
20. Rogers, K. , et al., *Three-dimensional UAV-based atmospheric tomography.* Journal of Atmospheric and Oceanic Technology, 2013. **30**(2): p. 336-344.
21. Wiens, T. , et al., *Turbulent flow sensing using acoustic tomography.* Proceedings of Innovations in practical Noise Control, 2009. **2009**.
22. Gregor, J. , et al., *Comparison of SIRT and SQS for regularized weighted least squares image reconstruction.* IEEE transactions on computational imaging, 2015. **1**(1): p. 44-55.
23. Hansen, P.C., *Discrete inverse problems: insight and algorithms*. Vol. 7. 2010: Siam, Philadelphia.
24. Jiang, M. , et al., *Convergence studies on iterative algorithms for image reconstruction.*

IEEE Transactions on Medical Imaging, 2003. **22**(5): p. 569-579.
25. Liu, S., et al., *Prior-online iteration for image reconstruction with electrical capacitance tomography.* IEE Proceedings-Science, Measurement and Technology, 2004. **151**(3): p. 195-200.
26. Kim, B.S., et al., *Electrical resistance imaging of two-phase flow using direct Landweber method.* Flow Measurement and Instrumentation, 2015. **41**: p. 41-49.
27. Rienstra, S.W. , et al., *An introduction to acoustics.* Eindhoven University of Technology, 2003. **18**: p. 19.
28. Li, S., et al., *Functional generalized inverse beamforming with regularization matrix applied to sound source localization.* Journal of Vibration and Control, 2016: http://dx.doi.org/10.1115/1.4032305.